Am J Physiol Cell Physiol 285: C1082–C1090, 2003.
First published July 2, 2003; 10.1152/ajpcell.00159.2003.

Intracellular stress tomography reveals stress focusing and structural anisotropy in cytoskeleton of living cells

Shaohua Hu,[1] Jianxin Chen,[1] Ben Fabry,[1] Yasushi Numaguchi,[2] Andrew Gouldstone,[1] Donald E. Ingber,[2] Jeffrey J. Fredberg,[1] James P. Butler,[1] and Ning Wang[1]

[1]*Physiology Program, Harvard School of Public Health, and* [2]*Vascular Biology Program, Departments of Surgery and Pathology, Children's Hospital and Harvard Medical School, Boston, Massachusetts 02115*

Submitted 23 April 2003; accepted in final form 26 June 2003

Hu, Shaohua, Jianxin Chen, Ben Fabry, Yasushi Numaguchi, Andrew Gouldstone, Donald E. Ingber, Jeffrey J. Fredberg, James P. Butler, and Ning Wang. Intracellular stress tomography reveals stress focusing and structural anisotropy in cytoskeleton of living cells. *Am J Physiol Cell Physiol* 285: C1082–C1090, 2003. First published July 2, 2003; 10.1152/ajpcell.00159.2003.—We describe a novel synchronous detection approach to map the transmission of mechanical stresses within the cytoplasm of an adherent cell. Using fluorescent protein-labeled mitochondria or cytoskeletal components as fiducial markers, we measured displacements and computed stresses in the cytoskeleton of a living cell plated on extracellular matrix molecules that arise in response to a small, external localized oscillatory load applied to transmembrane receptors on the apical cell surface. Induced synchronous displacements, stresses, and phase lags were found to be concentrated at sites quite remote from the localized load and were modulated by the preexisting tensile stress (prestress) in the cytoskeleton. Stresses applied at the apical surface also resulted in displacements of focal adhesion sites at the cell base. Cytoskeletal anisotropy was revealed by differential phase lags in *X* vs. *Y* directions. Displacements and stresses in the cytoskeleton of a cell plated on poly-L-lysine decayed quickly and were not concentrated at remote sites. These data indicate that mechanical forces are transferred across discrete cytoskeletal elements over long distances through the cytoplasm in the living adherent cell.

mechanical forces; deformation; focal adhesion; microfilament

HOW DO CELLS SENSE AND RESPOND to mechanical stresses applied at the cell surface? Despite ample evidence that mechanical forces and mechanotransduction are critical for many cell functions including growth, proliferation, protein synthesis, and gene expression (7, 20, 22), the specific mechanisms of mechanical force transmission remain elusive. Published reports show that forces applied at the cell surface via integrin receptors (but not via nonadhesion receptors) are transmitted to the cytoskeleton and nucleus (6, 23, 33) and that the cytoskeleton behaves as a prestressed network of discrete elements (29, 34, 35). These observations conflict with the classic view of the cell as a simple mechanical continuum (12, 15) but are consistent with the prestressed discrete network model (4, 28). These observations are also consistent with recent reports that apical fluid shear stresses produce a heterogeneous distribution of displacements and strain within the intermediate filament (IF) cytoskeleton (17–19). However, because those IF displacement measurements were carried out over minutes it is not clear whether the strain heterogeneity is due to a direct mechanical response or a biochemical remodeling response. Moreover, no cytoskeleton stress or phase lag distribution could be quantified with the fluid flow approach. Local heterogeneous mechanical properties of the cytoplasm have been detected by tracking Brownian motion of individual microinjected nanoparticles in the cytosol (32), but again this heterogeneity could be due to active transport or remodeling processes and it is not possible to separate cytoskeleton structural contribution from fluid cytosol contribution by this approach. We previously reported (34) visualization of yellow fluorescent protein (YFP)-mitochondria movements in response to a large cell surface deformation (5–7 μm) induced by a micropipette-displaced ligand-coated magnetic bead. However, no displacement fields, phase lags, or stress fields could be quantified in that study.

In the present study, we present a novel method of intracellular stress tomography that uses synchronous detection methods to compute stresses as well as displacements within the cytoskeleton in response to a small localized oscillatory load. We found that external load-induced displacements, stresses, and phase lags were concentrated at remote sites from the localized load.

METHODS

Cell culture and fluorescent protein delivery. Human airway smooth muscle cells were isolated from tracheal muscle obtained from lung transplant donors in conformance with the "Guiding Principles for Research Involving Animals and Human Beings" of the American Physiological Society and cultured by a previously published method (35). Adenovirus vectors were used to transiently infect YFP-cytochrome *c*

Address for reprint requests and other correspondence: N. Wang, Physiology Program, Harvard School of Public Health, 665 Huntington Ave., Boston, MA 02115 (E-mail: nwang@hsph.harvard.edu).

The costs of publication of this article were defrayed in part by the payment of page charges. The article must therefore be hereby marked "*advertisement*" in accordance with 18 U.S.C. Section 1734 solely to indicate this fact.

oxidase, green fluorescent protein (GFP)-caldesmon, or YFP-actin into the cells. After the cells (*passages 3–8*) reached 70–80% confluence, the adenovirus-containing YFP-mitochondria (or YFP-actin or GFP-caldesmon) were added at 150 μl/well (6-well dish) for 2 days. GFP-paxillin was transiently transfected into the cells with an electroporation method. The cells were plated sparsely on type I collagen-coated dishes or poly-L-lysine-coated dishes (both at 20 μg/ml) in serum-free medium overnight before experiments.

Application of localized loads and synchronous detection of displacements. We applied mechanical torques to cells in a dish under a microscope at 37°C. Ferromagnetic beads (4.5-μm diameter) coated with Arg-Gly-Asp (RGD)-containing peptides, specific ligands for integrin receptors, were bound to the apical surface of the adherent cells for 15 min. The beads were magnetized with a strong (1,000 G), short (<0.1 ms) magnetic field pulse oriented at the horizontal direction. A sinusoidally varying vertical magnetic "twisting" field was applied, and resulting bead translational displacements induced by bead rotation were determined by quantifying the bead center movement with an intensity-weighted center-of-mass algorithm (10). The phase-contrast images of the magnetic bead were recorded during oscillatory load application at 10 images per cycle before or after fluorescent images were taken. Lateral movements of the bead center that were synchronized with the input torque were analyzed as the bead displacements. The specific torque applied to the beads was calibrated by rotating beads in a viscosity standard (33). The mechanical specific torque of 90 Pa was applied at a fixed frequency of 0.3125 Hz about an axis in the *X* direction (10). This torque induced a peak-to-peak rotation of the magnetic microbead of ~5–15° (0.09–0.26 angular strain) that in turn produced a small local surface deformation (~0.2–0.6 μm) without gross distortion of the cell surface. The bead lateral movement was used to calculate the corresponding dynamic modulus (9, 24). Fluorescent image acquisition was phase locked to the twisting field such that 10 images were taken during one twisting cycle of 3.2 s. Thus the temporal resolution was 0.32 s. To reduce noise caused by spontaneous movements of mitochondria and other cytoskeleton structures, we often averaged images taken during the same twisting phase over a few to 10 cycles (10–30 s). The images were subdivided into arrays of 11 × 11 pixels (2.2 μm × 2.2 μm). The arrays overlapped by five pixels (1.0 μm). We computed the displacement field by comparing corresponding arrays between two images taken at different phases during the twisting cycle and by shifting the arrays of the second image by subpixel increments (10 nm) in the Fourier domain until the mean square differences of the pixel intensities between the shifted array and the corresponding array from the first image reached a minimum. The resolution of the displacement measurements was ~10 nm. Stress fields were computed from displacement fields with published methods (5, 31).

Characterization of displacement lumps. Lumps were defined as local maxima (within a 3-μm circle) of the displacement field, subject to the following constraints: a lump had to be >3 μm away from the bead center, it had to have an amplitude of >30 nm, and it had to have an amplitude 30% greater than that of its surrounding pixels. To prevent noise from erroneously being identified as lumps, we eliminated data with a signal-to-noise ratio of <3.

Finite-element analysis. A finite-element analysis with the multipurpose program ABAQUS (version 6.2, HKS Software, Pawtucket, RI) was performed to simulate displacements induced by twisting a magnetic bead in a continuum solid. The rigid bead was embedded 50% into the medium, and the medium thickness was two bead radii. The length and width of the medium were set to be infinite. The bead rotated by 6.5° in the *Z* direction, similar in magnitude to what was applied to living cells. The displacements of the solid in the *X-Y* plane at 0.5 radii above the bottom were computed. The bottom of the medium was fixed, and the mesh size was 0.2 μm. Poisson ratio was set to 0.49.

RESULTS AND DISCUSSION

Displacements and stresses in cells plated on extracellular matrix molecules are concentrated at remote sites and form discrete lumps. Intracellular displacements in response to stress were tracked by analyzing changes in the position of mitochondria in airway smooth muscle cells that were infected with an adenovirus that encodes YFP-cytochrome-*c* oxidase at the inner mitochondrial membrane. Mitochondria connect to microtubules (MTs) through the motor molecules kinesin and dynein (30) and are distributed throughout the entire cytoplasm, while being excluded from the actin-rich cortex and nucleus (34). Thus the fluorescent mitochondria can be used as fiducial markers to quantify cytoskeleton displacements that result from local mechanical loads applied via integrins (34). The focal plane of fluorescent images was ~2 μm above the cell base. Mitochondria position was tracked with a temporal resolution of 0.32 s and spatial resolution of displacements of 10 nm.

The displacements of mitochondria in the *X-Y* plane did not decay quickly away from the bead center (i.e., the localized load) in cells that were plated on extracellular matrix (ECM) molecules such as type I collagen. Appreciable displacements could be clearly detected >20 μm away from the bead center (Fig. 1, *A* and *B*, and Fig. 2), extending previous results obtained with large static deformation (34). The observed distribution of displacements of the mitochondria was not smooth but rather was concentrated and focused at distant sites in a discrete manner that could be described as "lumpy" (Fig. 2*A*). There were on average 3.5 lumps per cell ($n = 87$ cells, of which 13 cells had no lumps). Furthermore, the displacement amplitudes at the lump sites were still >50% of the maximum displacement at a distance of 24–27 μm from the bead center (Fig. 2*B*). The average maximum mitochondria displacement amplitude was 0.148 ± 0.013 μm (mean ± SE), and the average maximum lateral bead displacement was 0.346 ± 0.034 μm. In contrast, mitochondrial displacements induced by beads bound to nonadhesion receptors on the cell surface quickly decrease to zero just a few micrometers away from the beads (34). Finite-element analysis of the displacement field of a homogeneous continuum solid in response to a similar magnitude of bead rotation revealed that the magnitudes of displacements in the *X-Y* plane decayed rapidly and smoothly to <10% just 7 μm away from the load center (Fig. 2*B*). These displacement data from living cells represent a major departure from predictions from a homogeneous continuum solid.

Interfacial stresses between the cell and its substrate can be quantified by traction microscopy, a

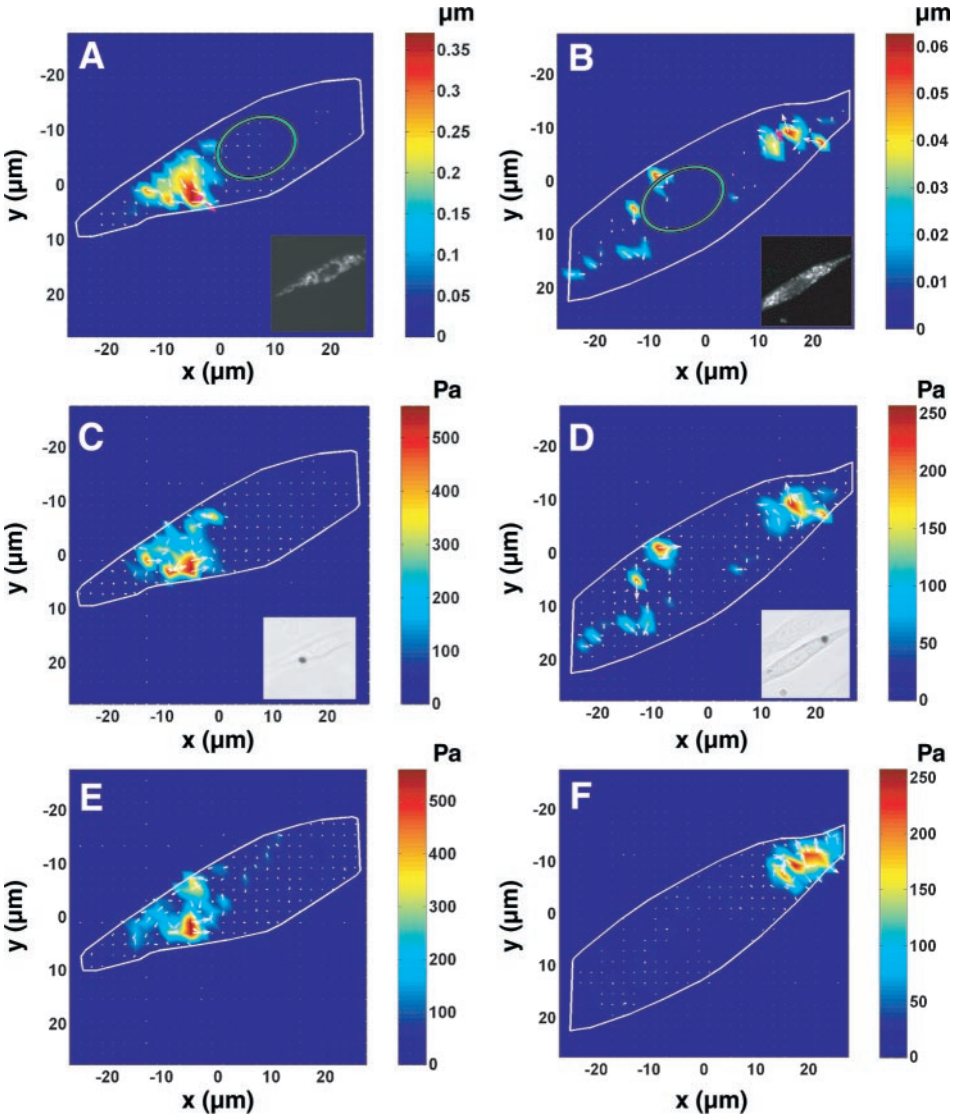

Fig. 1. Displacement and stress maps of living cells. *A* and *B*: maps of displacements of mitochondria of 2 individual cells under baseline conditions in response to a localized load applied with an Arg-Gly-Asp (RGD)-coated magnetic bead bound to the apical surface. *C* and *D*: corresponding stress maps computed from the displacement maps of the 2 cells in *A* and *B*. The white arrows represent the directions and relative magnitudes of mitochondria; the pink arrow in *A* and *B* represents the direction and relative magnitude of the bead center displacement. The color map represents the magnitudes of the mitochondria displacements or stresses. *Insets* in *A* and *B* are fluorescent images of the mitochondria. The mitochondria focal plane was 2 μm above the cell basal surface. *Insets* in *C* and *D* are phase-contrast images of corresponding cells (the black dot in each image is the magnetic bead). *E*: stress maps of the mitochondria 10 s after histamine treatment (10 μM). *F*: stress map 3 min after cytochalasin D (CytoD) treatment (1 μg/ml). Five other cells in histamine condition and three other cells in CytoD condition exhibited similar behaviors.

method that tracks movements of fluorescent beads embedded in an elastomeric gel just beneath the cell base (5, 8, 26, 31). In this study we adapted this approach to the interior of the cell by tracking movements of the YFP-mitochondria that are synchronized with the movement of the integrin-bound magnetic bead (i.e., the applied load). Using a modified Fourier transform traction cytometry (FTTC) method recently developed in our laboratory (5, 31), we computed an index of stress analogous to tractions acting on a plane (i.e., the focal plane of the fluorescent image) that would be required to generate the displacement fields such as those illustrated in Fig. 1, *A* and *B*. This traction field represents an index of the stress field inside the cell that acts in the *X*-*Y* direction at a cell height given by the focal plane, thereby making it possible to carry out "stress tomography." From the lateral bead displacements, we estimated the Young's modulus of the cell (10, 24), assuming a Poisson ratio of 0.48. Figure 1, *C* and *D*, shows the corresponding stress fields calculated from the mitochondrial displacement fields in Fig. 1, *A* and *B*. We found that stresses were concentrated and focused at discrete sites. Furthermore, stresses were still large at distances >20 μm away from the maximum stress, demonstrating long-distance force transmission to sites remote from the point of localized load application. Our observations are in sharp contrast to a previous finding in the cytoplasm of J774 macrophages that no induced displacement is detected at distances of ~1–2 μm away from the local force (2). The likely explanation is that in that study the particles were phagocytosed nonspecifically in the cytoplasm and thus no cytoskeleton displacement could be measured, although differences in cell types may also be partially responsible (normal human airway smooth muscle cells in our study and a mouse tumor macrophage cell line in that study).

Displacement and stress distribution patterns are modulated by prestress. The prestress that tenses the cytoskeleton is critical in determining cell shear stiffness and maintaining cell shape stability (34, 35). Here we explored the possibility that prestress might also

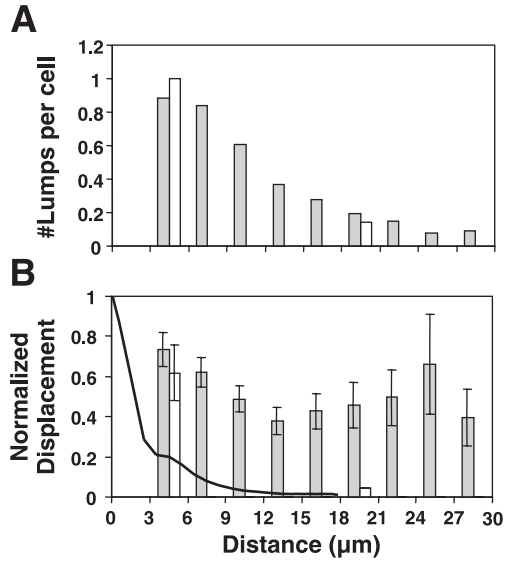

Fig. 2. Displacements are focused and lumpy. *A*: no. of displacement lumps per cell. *B*: normalized displacement amplitude at lump sites (amplitude divided by maximum amplitude) as a function of the distance from the load (bead) center. Data shown by gray bars are from the baseline condition; the average maximum mitochondria displacement amplitude was 0.148 ± 0.013 μm (mean ± SE). The solid line is the prediction from the finite element analysis of a continuum solid under a similar loading condition. On average there were 3.5 lumps/cell (n = 87 cells, of which 13 cells had no lumps). Lump displacement amplitudes at various distances (except those at 6–9 μm and at 24–27 μm) were significantly different ($P < 0.02$) from the lump amplitude at 3–6 μm. Data shown by open bars are from the CytoD condition (1 μg/ml for 5–10 min); the average maximum mitochondria displacement amplitude was 0.297 ± 0.113 (mean ± SE). On average there were 1.1 lumps/cell (n = 7 cells). The lump (open bar) at 18–21 μm was probably due to incomplete disruption of actin bundles.

play an important role in force transmission through the cytoplasm by tensing the cytoskeleton lattice. This mode of force transmission differs from conventional models that consider only the rheological properties of the cytoskeleton (3, 11, 12, 15). To determine to what degree the prestress might be able to modulate these external load-induced stress concentrations in the cytoskeleton, we increased the prestress by activating the cell with histamine, a contractile agonist that increases cytoskeleton tension by activating actomyosin interactions. Stress patterns changed significantly within 10 s of drug treatment. For example, in the cell shown in Fig. 1*E*, two stress lumps to the left of the peak stress disappeared and two stress lumps at the top merged into one large lump, in the absence of any visible cell shape change. Although this change in stress patterns could be due to histamine's effect on other biochemical signaling pathways, our previous studies in these cells (10, 35) show that both stiffness and prestress exhibit dose-dependent increases in response to histamine, suggesting that it is most likely due to elevation of contractile forces. Because actin microfilaments (MFs) are the primary component of the cytoskeleton that carries the prestress, we reasoned that disrupting actin lattice integrity might alter the stress distribution pattern if prestress were important. Indeed, disrupting actin MF lattice integrity with cytochalasin D led to an almost complete abolishment of stress lumps, while limiting large local stresses to the vicinity of the bead (Fig. 1*F*). Cytochalasin D abolished most displacement lumps at remote sites such that the remaining lumps were located <6 μm from the load center (Fig. 2). This result suggests that integrity of the actin lattice and the prestress carried by these actin MFs are important in modulating long-distance transfer and stress concentration in the cytoskeleton in response to a localized load. Disrupting MTs with nocodazole and intermediate filaments with calyculin also resulted in significant changes in displacement and stress distributions (Hu S and Wang N, unpublished results), suggesting that all three cytoskeleton filament systems contribute to stress propagation, although actin filaments appear to be the most important.

To more directly determine whether cytoskeleton prestress might play a role in modulating stress concentrations, we infected the cells with an adenovirus containing GFP-caldesmon (16, 25). Caldesmon, a component of the contractile apparatus that binds actin, myosin, and tropomyosin, inhibits cytoskeleton tension in cells by interfering with ATPase activity of actomyosin in a Ca^{2+}-calmodulin-dependent manner (16). When expressed, GFP-caldesmon decorated the actin MFs, and thus the fluorescent images of these cells could be used to directly track displacements of MFs under mechanical loads. Cells infected with a low level of caldesmon showed a 50% decrease in prestress, although they did not display any obvious alteration in cell shape, stress fibers, or focal adhesions (25). As a control, cells expressing YFP-actin were analyzed in parallel. In response to the oscillatory load, a cell with YFP-actin displayed numerous lumps of displacements and stresses (at a focal plane of ~1 μm from the cell base) (Fig. 3, *A* and *B*). In contrast, under the same load, a cell expressing a low level of GFP-caldesmon with normal-appearing stress fibers exhibited much fewer displacement and stress lumps (Fig. 3, *C* and *D*). The stress distribution patterns also were altered when Rho-associated kinase (ROCK)-dependent cytoskeleton tension was inhibited in cells by treatment with Y-27632 (S. Hu and N. Wang, unpublished results). Importantly, the inhibitory effects of caldesmon on the number of displacement and stress lumps were reversed by treatment with calcium ionophore A-23187 (Fig. 3, *E* and *F*), which was previously shown to reverse the inhibitory effects of caldesmon on actomyosin-based contraction (16). The increase in the number of stress lumps after drug treatment occurred before any visible increase in the number of stress fibers, suggesting that the observed effects were likely due to the effects on cytoskeleton prestress. It is interesting that a few displacements and stress lumps overlapped with the nucleus in both the control cell (Fig. 3, *A* and *B*) and the calcium ionophore-treated GFP-caldesmon cell (Fig. 3, *E* and *F*). This finding suggests that intranuclear structures may be deformed by these concentrated stresses, as previously demonstrated when

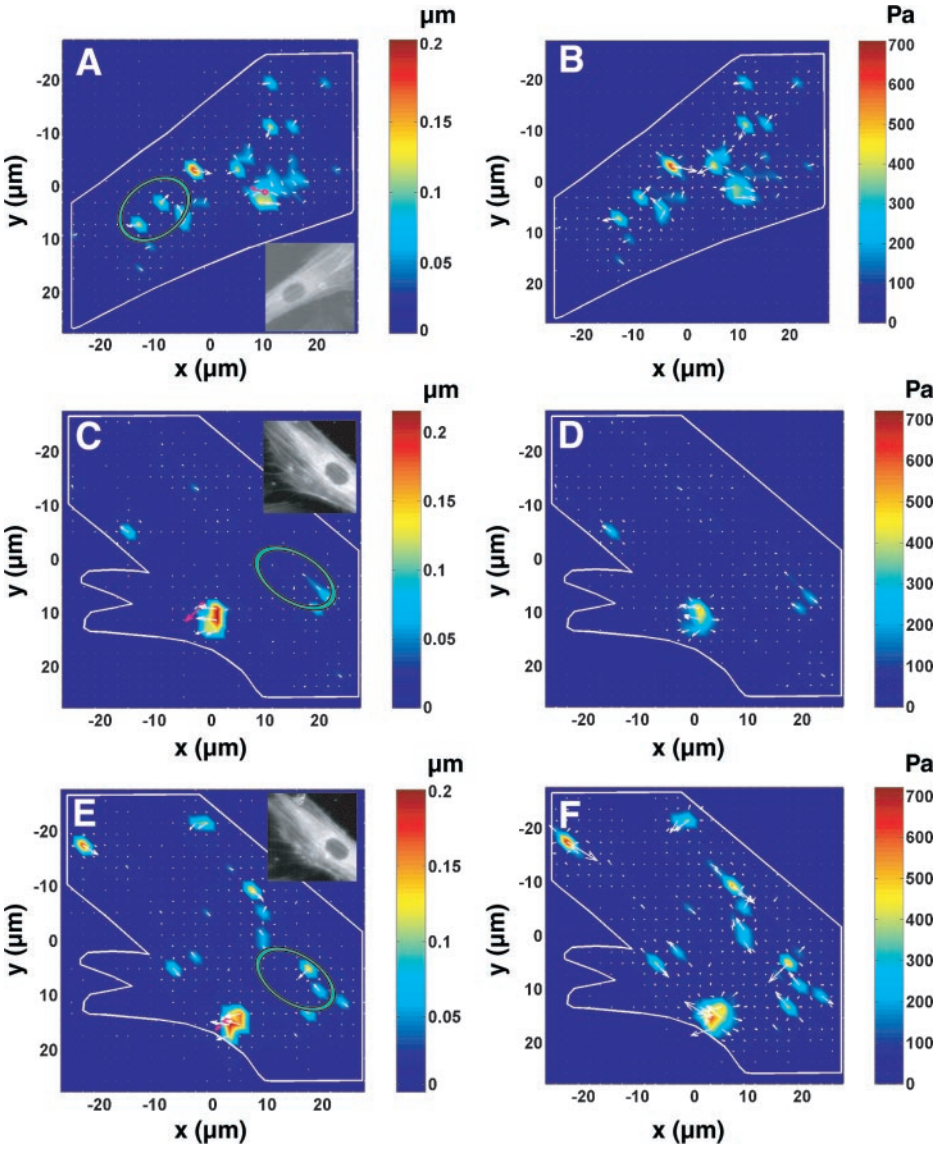

Fig. 3. Actin cytoskeleton displacement and stress patterns are modulated by prestress. *A* and *B*: displacement (*A*) and stress (*B*) maps of a control yellow fluorescent protein (YFP)-actin cell. The focal plane was ~1 μm above the cell base. Displacement field images (*C*, *E*) and stress field images (*D*, *F*): cell infected with a low level of green fluorescent protein (GFP)-caldesmon before (*C*, *D*) and after (*E*, *F*) treatment with calcium ionophore A-23187 (5 μg/ml for 10 min), an inhibitor of caldesmon. The pink arrow represents the direction and the magnitude of the bead lateral displacement. Insets in *A*, *C*, and *E* are fluorescent images of the corresponding cells, showing patterns of stress fibers. Green ellipses represent the nuclei of the cells. Four other cells exhibited similar behaviors.

gross distortion of the cell (~10- to 20-μm deformation) was produced through integrin-bound micropipettes (23). The finding that localized stress concentrations were also observed in GFP-caldesmon cells and YFP-actin cells confirms that the similar results obtained with YFP-mitochondria cells were not due to artifacts relating to spontaneous movements and/or out-of-focal-plane mitochondria or changes in dynamic associations between mitochondria and MTs.

Stresses applied at cell apex are transmitted to focal adhesions at cell base. Actin stress fibers that generate and bear mechanical stresses are anchored at the cell base to underlying ECM through integrin receptors within localized focal adhesions. We therefore asked whether the stresses applied at the apical surface were transmitted to focal adhesions at the basal surface, which were previously shown to transmit internal cytoskeleton contractile forces to the external substrate (1). Cells transfected with GFP-paxillin, a focal adhesion protein, exhibited streaklike focal contacts containing GFP (Fig. 4, *A* and *B*). Application of a localized oscillatory load at the apical cell surface via integrins resulted in focused displacements at the paxillin-labeled adhesions at the cell base (Fig. 4, *C* and *D*) and concentrated stresses on these focal adhesions (Fig. 4, *E* and *F*). Importantly, these induced displacements at the focal adhesions were propagated to the substrate just beneath the cells, as quantified by tracking red fluorescent bead movements in a polyarylamide gel on which the cells spread (S. Hu and N. Wang, unpublished results). Thus these results unequivocally demonstrate that local stresses applied at the apical cell surface are transmitted through the cytoplasm and to the underlying substrate via discrete basal focal adhesions, where stresses are focused and concentrated. The fact that these focal adhesion displacements occurred at many sites inside the cytoplasm is not consistent with the hypothesis that the membrane cortex is the primary pathway for force propagation, as proposed in past studies (12, 13, 15). Rather, it is consis-

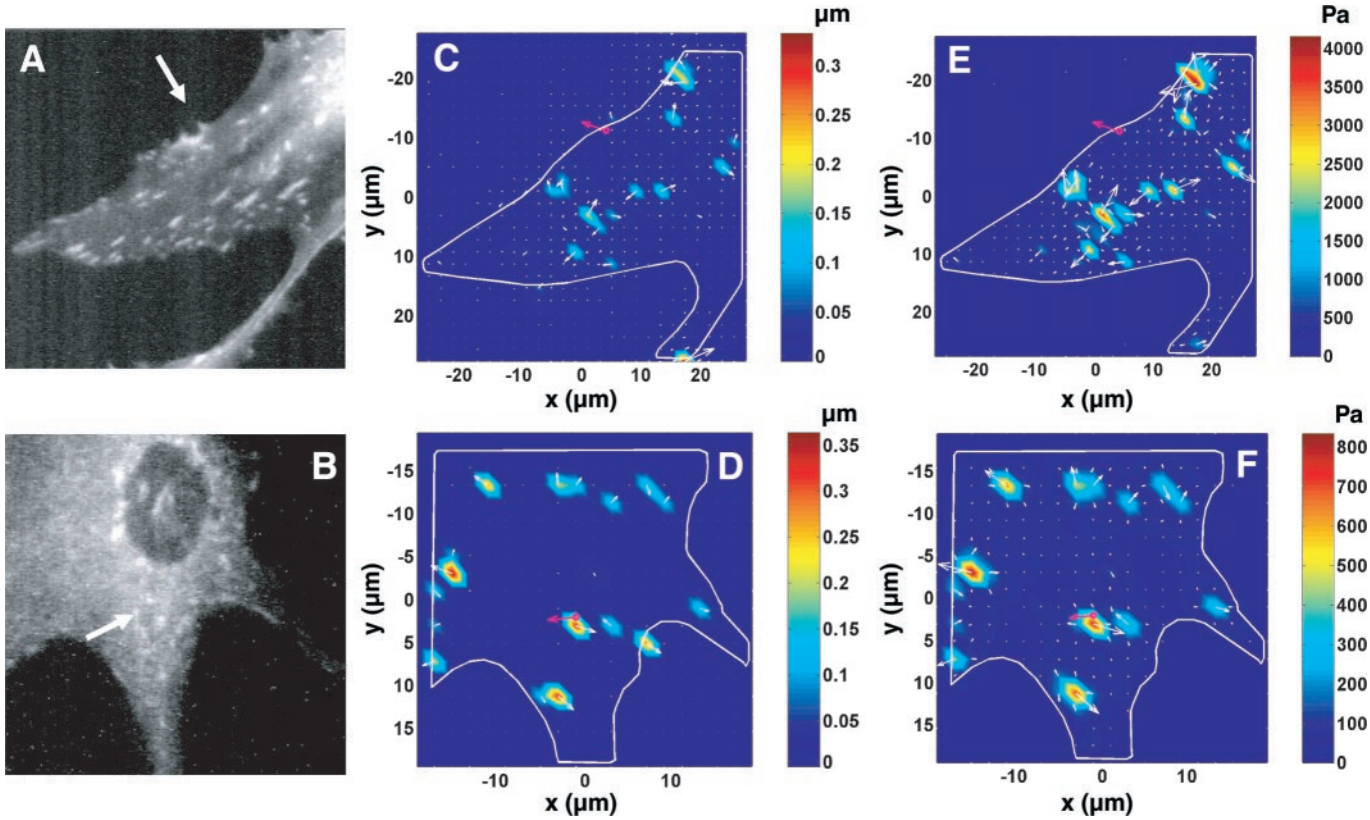

Fig. 4. Stress applied at cell apex results in displacements at basal focal adhesions. The cells were plated on type I collagen-coated rigid dishes. *A* and *B*: fluorescent images of 2 individual cells (white arrows point to the position of the magnetic beads, the center of the applied load). *C* and *D*: induced displacements of GFP-paxillin synchronized with the applied load. *E* and *F*: computed stress maps. The pink arrow represents the direction and relative magnitude of the magnetic bead center displacements (the applied load). The colors and white arrows represent the magnitudes and directions of the induced displacements or stresses. Three other cells showed similar behaviors.

tent with the notion that tensed discrete molecular filament networks transmit mechanical forces between focal adhesions and the remaining structural elements of the cell (29, 34, 35). Interestingly, not all focal adhesions were displaced to the same extent; some basal focal adhesions under the site of the localized load displaced little (Fig. 4*C*). This provides additional evidence that localized stresses applied to the cell apical surface are not transmitted smoothly and homogeneously through the cytoskeleton. Although we still do not know the specific structural basis for the focusing of these displacements and stresses, our data show that focal adhesions, cytoskeleton prestress, and all three cytoskeleton filament systems play important roles. Our data are consistent with the finding that IFs in living endothelial cells displace in a heterogeneous manner in response to uniform apical shear stress that leads to strain focusing, including regions at the cell base (18) and the finding that local Brownian motions of microinjected nanoparticles are heterogeneous in the cytoplasm of living cells (32). Importantly, a major advantage of the stress tomography approach described here is that we quantify fluorescent images at a fast rate of 3 Hz; together with synchronous detection, this can exclude most, if not all, of the contribution of active biochemical processes, such as cytoskeleton remodeling. Some might argue that the stress concentrations we demonstrated could be explained by local cytoskeleton stiffness variations of continuum models, but they still could not explain long-distance load transfer (Figs. 1, 2, and 3) and the concentrated displacements at the focal adhesions (Fig. 4).

Cytoskeleton dissipative behavior is also heterogeneous and lumpy. It is well known that living cells behave mechanically as viscoelastic materials, but the mechanisms governing friction and energy dissipation in the cytoskeleton are unclear (9); moreover, it has been suggested that these processes might be the origins of local remodeling and mechanotransduction (9). To better characterize frictional stresses we quantified the phase lag between mitochondria/MF movements and the applied oscillatory torque throughout the cell body. Phase lags from cells in both *X* and *Y* directions were found to be quite heterogeneous; local phase lags ranged from 0° (purely elastic) to 50° (viscoelastic) (Fig. 5). The phase lags were site specific in all cells, both locally at the site of force application and distally at discrete regions through the cytoplasm. Moreover, the distribution of the phase lags was altered and the average phage lag decreased when the cytoskeleton prestress was increased by histamine (Hu S and Wang N, unpublished results). Overlapping the stress map

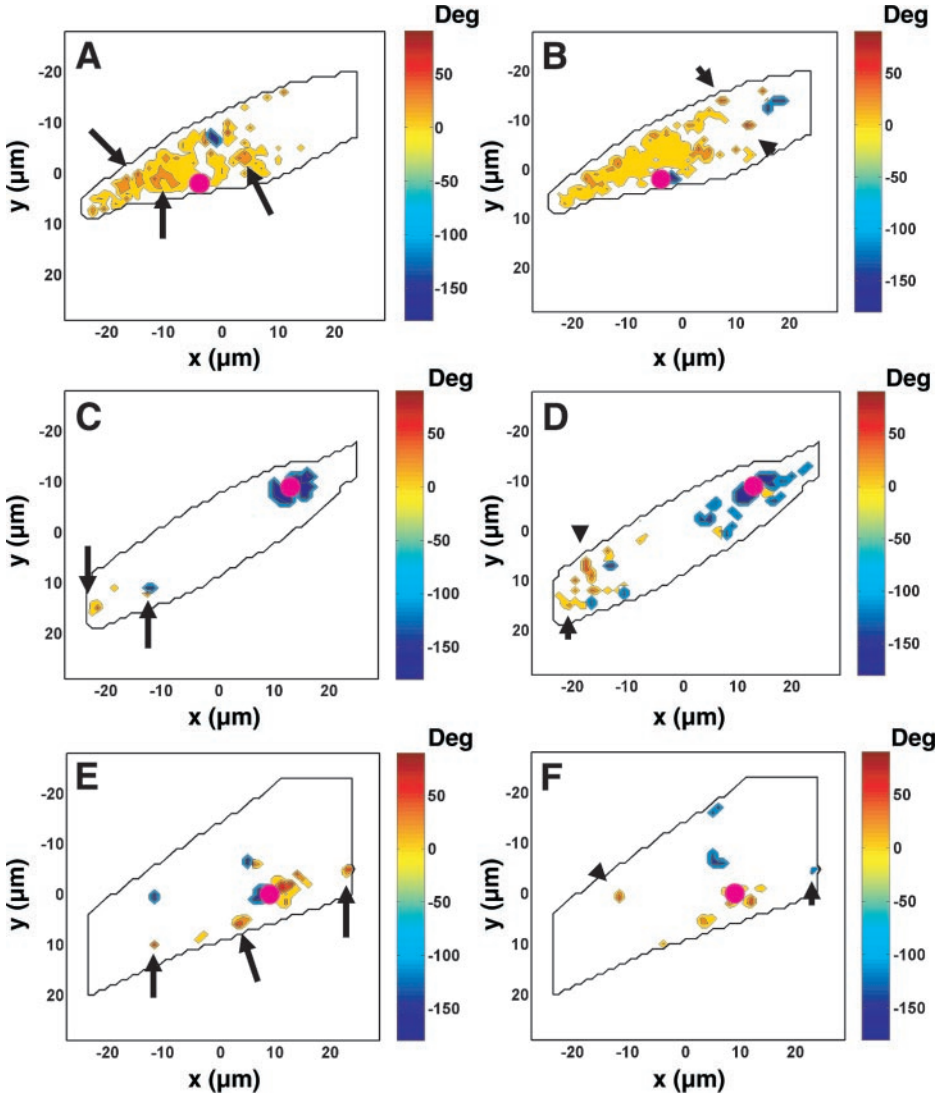

Fig. 5. Phase lags are heterogeneous and lumpy. Distribution of phase shifts (phase lags) between mitochondria or microfilament displacements and the applied load in 3 individual cells under baseline conditions. *A*, *C*, and *E*: phase lag map in the *X* direction. *B*, *D*, and *F*: phase lag map in the *Y* direction. *A* and *B* correspond to the cell in Fig. 1, *A* and *C*; *C* and *D* correspond to the same cell in Fig. 1, *B* and *D*; *E* and *F* correspond to the same cell in Fig. 2, *A* and *B*. Colors represent magnitudes of the phase lags in degrees (blue represents those structures that were almost 180° out of phase with the input load). The pink dot represents the position of the magnetic bead, the site of the localized load. White areas are the sites with poor signal-to-noise ratio (<3), and thus no phase lag information was analyzed. Black arrows point to large phase lags that did not overlap with high-stress concentrations. Black arrowheads point to phase lags in the *Y* direction that were different from those in the *X* direction.

with the phase lag map of the same cell (Fig. 1*C* with Fig. 5, *A* or *B*; Fig. 1*D* with Fig. 5, *C* or *D*; Fig. 2*B* with Fig. 5, *E* or *F*), we found that the site of the local maximum stress did not necessarily coincide with the site of the largest phase lag (see arrows in Fig. 5, *A*, *C*, and *E*). Furthermore, phase lags in the *X* and *Y* directions at the same location were sometimes different (see arrowheads in Fig. 5, *B*, *D*, and *F*), suggesting structural anisotropy in the cytoskeleton lattice.

Cells plated on poly-L-lysine do not exhibit long-distance force transfer behavior. To further explore the effects of focal adhesions on the load-induced displacement and stress distribution patterns, we plated cells on poly-L-lysine coated dishes rather than on type I collagen as shown in the above-described experiments. Consistent with the previous finding that cells plated on poly-L-lysine do not form focal adhesions (27), our smooth muscle cells formed almost no stress fibers after being plated overnight in serum-free medium (not shown). Although these cells adhered and spread very well, just like the cells on ECM molecules, they lost the elongated shape of airway smooth muscle cells and assumed pancakelike shapes (Fig. 6, *A* and *B*). Quantification of displacements and stresses revealed that they decayed quickly in space and were only localized to the vicinity of the load center (Fig. 6, *C* and *D*), in sharp contrast to the displacement and stress distribution patterns in the cells plated on type I collagen-coated dishes (see Fig. 1). On average there were only 1.2 lumps per cell (Fig. 6*C*; $n = 20$ cells, of which 9 cells had no lumps) compared with 3.5 lumps per cell for cells on type I collagen (Fig. 2). The number of lumps per cell decreased by 66% and the amplitudes of these lumps decreased very quickly from the load center (Fig. 6, *C* and *D*). These data suggest that the presence of focal adhesions and stress fibers is primarily responsible for the formation of these displacement lumps. It is possible that the remaining cytoskeleton filament systems (e.g., MTs, IFs, thin MFs) are responsible for generating the remaining lumps. Furthermore, the average maximum mitochondria displacement amplitude was only 0.079 ± 0.021 μm (mean ± SE), much lower than that of 0.148 ±0.013 μm for cells on type I collagen ($P < 0.05$), indicating that for the same applied

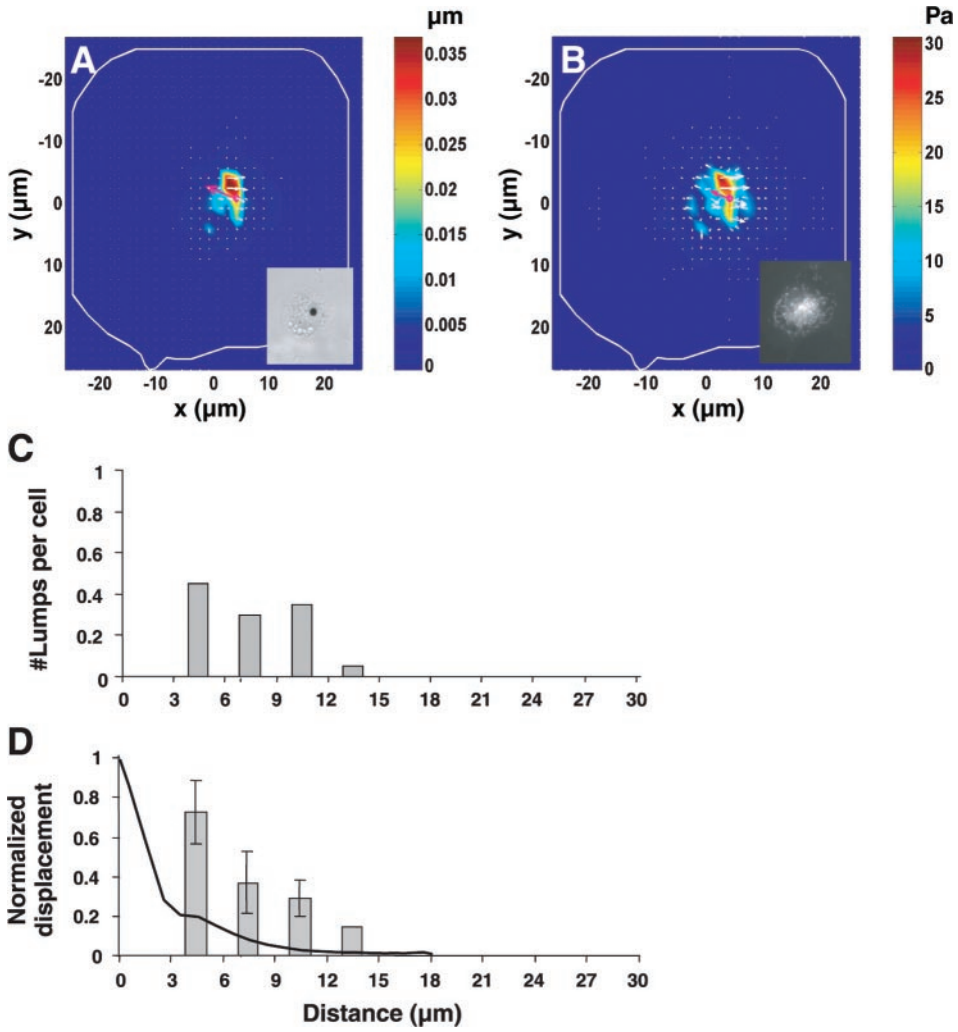

Fig. 6. Displacement and stress distribution in cells plated on poly-L-lysine coated dishes. *A* and *B*: displacement field and stress field of a representative cell. *Insets* in *A* and *B* are phase-contrast image and mitochondria fluorescent image. *C* and *D*: no. of displacement lumps per cell (*C*) and normalized displacement amplitude at lump sites (*D*), both as a function of the distance from the load center. The average maximum mitochondria displacement amplitude was 0.079 ± 0.021 μm (mean ± SE). Solid line is the prediction from the finite-element analysis of a continuum solid under a similar loading condition. There were on average 1.2 lumps/cell (n = 20 cells, of which 9 cells had no lumps).

load, the cytoskeleton displacements were much smaller. Interestingly, the average maximum lateral bead displacement in cells plated on poly-L-lysine was 0.827 ± 0.150 μm, much higher than that of 0.346 ± 0.034 μm for cells on type I collagen ($P < 0.01$). Hence these cells were much less stiff than those cells on ECM molecules (for a given load, the higher the bead displacement, the lower the stiffness). Because deep cytoplasmic cytoskeleton displacements were smaller and the surface deformation was larger, this suggests that the membrane cortex might balance much of the applied load in cells on poly-L-lysine. All these data demonstrate that, besides the degree of cell attachment and the extent of cell spreading (cells on both type I collagen and poly-L-lysine attached and spread very well), the existence of basal focal adhesions and stress fibers strongly influences displacement and stress distribution patterns in response to a small localized load. It remains to be seen whether cells that are plated on the same kind of ECM molecules but assume different shapes (i.e., elongated vs. round) would exhibit different force transmission behaviors.

Together, these results demonstrate the power of stress tomography to quantify stress distributions within the cytoskeleton of a living cell in response to a localized load applied at the apical surface. Our data reveal a highly heterogeneous pattern of long-distance force transfer and an associated focusing of displacements and stresses to discrete sites throughout the cytoskeleton, to the nucleus, and to basal focal adhesions. The long-distance stress transfer patterns are strongly dependent on focal adhesions and stress fibers, modulated by cytoskeleton prestress, and influenced by all three cytoskeleton filament systems. The specific molecular structural basis for these displacements and stress concentrations remains to be determined; however, these findings are consistent with the cellular transmission of forces by a tensed cable network model (4, 20, 21, 28, 29, 34, 35) and might be partially accounted for by preferential connections between the load site and the lump site via long stress-bearing filaments. A recent report that converging F-actin bundles in migrating cells promote associated MT buckling and breakage (14) raises the possibility that these concentrated MF-MT interactions could be the potential sites for stress focusing. A detailed three-dimensional map of the displacement/stress field and a three-dimensional structural map of stress fibers/F-

actin bundles and MTs should help elucidate the structural basis of these stress concentrations. Nevertheless, our findings could open the way for better understanding of the mechanisms of intracellular force transmission and transduction in living cells in response to external mechanical stimuli.

We thank M. Montoya for help with transfection of GFP-paxillin. We thank D. Stamenovic for reviewing the manuscript and R. Panettieri for providing the cells.

DISCLOSURES

This work was supported by National Heart, Lung, and Blood Institute Grant HL-33009 and National Aeronautics and Space Administration Grants NAG2-1509 and NAG2-1501.

REFERENCES

1. **Balaban NQ, Schwarz US, Riverline D, Goichberg P, Tzur G, Sabanay I, Mahalu D, Safran S, Bershadsky A, Addadi L, and Geiger B.** Force and focal adhesion assembly: a close relationship studied using elastic micropatterned substrates. *Nat Cell Biol* 3: 466–472, 2001.
2. **Bausch AV, Moller W, and Sackmann E.** Measurement of local viscoelasticity and forces in living cells by magnetic tweezers. *Biophys J* 76: 573–579, 1999.
3. **Bausch AV, Ziemann F, Boulbitch AA, Jacobson K, and Sackmann E.** Local measurements of viscoelastic parameters of adherent cell surfaces by magnetic bead micro-rheometry. *Biophys J* 75: 2038–2049, 1998.
4. **Budiansky B and Kimmel E.** Elastic moduli of lungs. *J Appl Mech* 54: 351–358, 1987.
5. **Butler JP, Tolic-Norrelykke IM, Fabry B, and Fredberg JJ.** Estimating traction fields, moments, and strain energy that cells exert on their surroundings. *Am J Physiol Cell Physiol* 282: C595–C605, 2002.
6. **Choquet DE, Felsenfeld DE, and Sheetz MP.** Extracellular matrix rigidity causes strengthening of integrin-cytoskeleton linkages. *Cell* 88: 39–48, 1998.
7. **Davies PF.** Flow-mediated endothelial mechanotransduction. *Physiol Rev* 75: 519–560, 1995.
8. **Dembo M and Wang YL.** Stresses at the cell-to-substrate interface during locomotion of fibroblasts. *Biophys J* 76: 2307–2316, 1999.
9. **Fabry B, Maksym GN, Butler JP, Glogauer M, Navajas D, and Fredberg JJ.** Scaling the microrheology of living cells. *Phys Rev Lett* 87: 148102, 2001.
10. **Fabry B, Maksym GN, Shore SA, Moore PE, Panettieri RA Jr, Butler JP, and Fredberg JJ.** Time course and heterogeneity of contractile responses in cultured human airway smooth muscle cells. *J Appl Physiol* 91: 986–994, 2001.
11. **Forgacs G.** On the possible role of cytoskeletal filamentous networks in intracellular signaling: an approach based on percolation. *J Cell Sci* 108: 2131–2143, 1995.
12. **Fung YC and Liu SQ.** Elementary mechanics of the endothelium of blood vessels. *J Biomech Eng* 115: 1–12, 1993.
13. **Gudi S, Nolan JP, and Frangos JA.** Modulation of GTPase activity of G proteins by fluid shear stress and phospholipid composition. *Proc Natl Acad Sci USA* 95: 2515–2519, 1998.
14. **Gupton SL, Salmon WC, and Waterman-Storer CM.** Converging populations of F-actin promote breakage of associated microtubules to spatially regulate microtubule turnover in migrating cells. *Curr Biol* 12: 1891–1899, 2002.
15. **Heidemann SR, Kaech S, Buxbaum RE, and Matus A.** Direct observations of the mechanical behaviors of the cytoskeleton in living fibroblasts. *J Cell Biol* 145: 109–122, 1999.
16. **Helfman DM, Levy ET, Berthier C, Shtutman M, Riverline D, Grosheva I, Lachish-Zalait A, Elbaum M, and Bershadsky AD.** Caldesmon inhibits nonmuscle cell contractility and interferes with the formation of focal adhesions. *Mol Biol Cell* 10: 3097–3112, 1999.
17. **Helmke BP, Goldman BP, and Davies PF.** Rapid displacement of vimentin intermediate filaments in living endothelial cells exposed to flow. *Circ Res* 86: 745–752, 2000.
18. **Helmke BP, Rosen AB, and Davies PF.** Mapping mechanical strain of an endogenous cytoskeletal network in living endothelial cells. *Biophys J* 84: 2691–2699, 2003.
19. **Helmke BP, Thakker DB, Goldman RD, and Davies PF.** Spatiotemporal analysis of flow-induced intermediate filament displacement in living endothelial cells. *Biophys J* 80: 184–194, 2001.
20. **Ingber DE.** Tensegrity: the architectural basis of cellular mechanotransduction. *Annu Rev Physiol* 59: 575–599, 1997.
21. **Ingber DE.** Tensegrity I. Cell structure and hierarchical systems biology. *J Cell Sci* 116: 1157–1173, 2003.
22. **Janmey PA.** The cytoskeleton and cell signaling: components, localization, and mechanical coupling. *Physiol Rev* 78: 763–781, 1998.
23. **Maniotis AJ, Chen CS, and Ingber DE.** Demonstration of mechanical connections between integrins, cytoskeletal filaments and nucleoplasm that stabilize nuclear structure. *Proc Natl Acad Sci USA* 94: 849–854, 1997.
24. **Mijailovich S, Kojic M, Zivkovic M, Fabry B, and Fredberg JJ.** A finite model of cell deformation during magnetic bead twisting. *J Appl Physiol* 93: 1429–1436, 2002.
25. **Numaguchi Y, Huang S, Polte TR, Eichler GS, Wang N, and Ingber DE.** Caldesmon-dependent switching between capillary endothelial cell growth and apoptosis through modulation of cell shape and contractility. *Angiogenesis*. In press.
26. **Pelham RJ Jr and Wang YL.** Cell locomotion and focal adhesions are regulated by substrate flexibility. *Proc Natl Acad Sci USA* 94: 13661–13665, 1997.
27. **Riverline D, Zamir E, Balaban NQ, Schwarz US, Ishizaki T, Narumiya S, Kam Z, Geiger B, and Bershadsky AD.** Focal contacts as mechanosensors: externally applied local mechanical force induces growth of focal contacts by an mDia1-dependent and ROCK-independent mechanism. *J Cell Biol* 153: 1175–1185, 2001.
28. **Stamenovic D, Fredberg JJ, Wang N, Butler JP, and Ingber DE.** A microstructural approach to cytoskeletal mechanics based on tensegrity. *J Theor Biol* 181: 125–136, 1996.
29. **Stamenovic D, Mijailovich SM, Tolic-Norrelykke IM, Chen J, and Wang N.** Cell prestress. II. Contribution of microtubules. *Am J Physiol Cell Physiol* 282: C617–C624, 2002.
30. **Tanaka Y, Kanai Y, Okada Y, Nonaka S, Takeda Harada AS, and Hirokawa N.** Targeted disruption of mouse conventional kinesin heavy chain kif5B results in abnormal perinuclear clustering of mitochondria. *Cell* 26: 1147–1158, 1998.
31. **Tolić-Nørrelykke IM, Butler JP, Chen J, and Wang N.** Spatial and temporal traction response in human airway smooth muscle cells. *Am J Physiol Cell Physiol* 283: C1254–C1266, 2002.
32. **Tseng Y, Kole TP, and Wirtz D.** Micromechanical mapping of live cells by multiple-particle-tracking microrheology. *Biophys J* 83: 3162–3176, 2002.
33. **Wang N, Butler JP, and Ingber DE.** Mechanotransduction across the cell surface and through the cytoskeleton. *Science* 260: 1124–1127, 1993.
34. **Wang N, Naruse K, Stamenovic D, Fredberg JJ, Mijailovich SM, Tolic-Norrelykke IM, Polte T, Mannix R, and Ingber DE.** Mechanical behavior in living cells consistent with the tensegrity model. *Proc Natl Acad Sci USA* 98: 7765–7770, 2001.
35. **Wang N, Tolic-Norrelykke IM, Chen J, Mijailovich SM, Butler JP, Fredberg JJ, and Stamenovic D.** Cell prestress. I. Stiffness and prestress are closely associated in adherent contractile cells. *Am J Physiol Cell Physiol* 282: C606–C616, 2002.